Structured Water Molecules on Membrane Proteins Resolved by Atomic Force Microscopy

Shinichiro Ido,[†] Kei Kobayashi,[†] Noriaki Oyabu,[†] Yoshiki Hirata,[§] Kazumi Matsushige,[†] and Hirofumi Yamada[*,†]

[†]Department of Electronic Science and Engineering, Kyoto University,

Kyoto-Daigaku-Katsura, Nishikyo, Kyoto, 615-8510, Japan

[§]National Institute of Advanced Industrial Science and Technology,

1-1 Umezono, Tsukuba, Ibaraki, 305-8566, Japan

[*]Hirofumi Yamada (corresponding author)

Department of Electronic Science and Engineering, Kyoto University

Kyoto-Daigaku-Katsura, Nishikyo, Kyoto, 615-8510, Japan

E-mail: h-yamada@kuee.kyoto-u.ac.jp

Phone: +81-75-383-2307, Fax: +81-75-383-2308

ABSTRACT

Water structuring on the outer surface of protein molecules called the hydration shell is essential as well as the internal water structures for higher-order structuring of protein molecules and their biological activities *in vivo*. We now show the molecular-scale hydration structure measurements of native purple membrane patches composed of proton pump proteins by a non-invasive three-dimensional force mapping technique based on frequency modulation atomic force microscopy. We successfully resolved the ordered water molecules localized near the proton uptake channels on the cytoplasmic side of the individual bacteriorhodopsin proteins in the purple membrane. We demonstrate that the three-dimensional force mapping can be widely applicable for molecular-scale investigations of the solid-liquid interfaces of various soft nanomaterials.

KEYWORDS

atomic force microscopy, force mapping, bacteriorhodopsin, protein, hydration

Structured water molecules around protein molecules are closely related to their structures and functions[1,2]. Protein hydration is essential for the protein molecules folding into higher-order structures by water-mediated interactions such as electrostatic interactions and hydrogen-bonding interactions. Dehydration of the protein molecules often unfavorably affects their biological activities. For example, the hydrogen-bond network of water molecules within transmembrane proteins plays crucial roles in the ion transfer through the biological membrane[3]. Bacteriorhodopsin (bR) is a transmembrane protein that serves as a light-driven proton pump[4,5]. The membrane patches containing bR molecules are called purple membranes (PM)[6], which can be easily isolated from the cell membrane of archaea *Halobacterium salinarum*. In the PM, the bR trimers form two-dimensional (2D) hexagonal crystals with a lattice constant of 6.2 nm. Electron crystallography of the PM first revealed that the bR molecule is composed of seven transmembrane alpha helices[7]. Since then, the atomic structures of bR and its biological function have been extensively studied[8,9] and bR has been a reference protein for understanding the structure-function correlation of general membrane proteins. Since the proton uptake and release occur at the bR–water interfaces, the local hydration structures on the protein surface is very important for understanding the proton translocation mechanism of bR. However, little is known about the molecular-scale hydration structures on the bR surface due to the lack of experimental methods. In this study, we used atomic force microscopy (AFM)[10] for measuring the distribution of water molecules

on the bR surface.

AFM is one of the few real-space imaging techniques that allows us to visualize the surface structures of biomolecules in solutions[11,12]. Previously, sub-molecular-scale structures and the dynamics of bR have been directly imaged in aqueous solutions by AFM[13,14]. We developed atomic resolution frequency modulation AFM (FM-AFM)[15] operated in liquid environments[16] and demonstrated 2D and 3D force mapping measurements using the FM-AFM for visualizing the spatial distribution of water molecules namely the hydration strucrtures[17-24] and electric double layer force[22,25,26]. Figure 1 shows a schematic diagram of the 3D frequency shift mapping by FM-AFM. In FM-AFM, interaction forces between the AFM tip and a sample are measured as the resonance frequency shift (Δf) of a cantilever while the cantilever is self-vibrated at its resonance frequency (f_0). The positive and negative frequency shifts from f_0 correspond to repulsive or attractive forces, respectively. In the 3D Δf mapping, the Δf versus distance curve measurements in the z-direction were repeated at every scanning pixel in the x–y plane. To prevent a hard contact of the AFM tip with the sample for the non-invasive measurement, an upper limit of the frequency shift (Δf threshold) regulated the maximum indentation force; once the Δf threshold was exceeded upon approaching, the AFM tip was immediately retracted from the sample. The sensitivity of the frequency shift detection, eventually the force sensitivity, is enhanced when the oscillation amplitude is set to the same order as the decay length of the interaction forces between the tip and sample, since

the frequency shift is roughly proportional to the weighted integral of the force derivative during an oscillation period[27]. Therefore in the hydration structure measurement using FM-AFM in aqueous solutions, the oscillation amplitude should be set as small as the size of the water molecule otherwise the hydration structure is not detected as the frequency shift.

Prior to the 3D Δf mapping, we obtained FM-AFM topographic images of the cytoplasmic side of the PM adsorbed onto a mica substrate in solution (Figure 2a–b). These images were taken with the oscillation amplitude of 0.5 nm, namely, 1.0 nm peak-to-peak. It should be noted that this is the oscillation amplitude optimized for high-resolution imaging. We hereafter refer to this condition as the large amplitude condition. In Figure 2b, the white circle indicates an individual bR trimer in the PM, as modeled in Figure 2c,d based on a crystallographic study[28]. The Chimera package (RBVI, University of California, San Francisco) was used to generate the molecular drawing[29]. The three bright spots of each bR trimer correspond to three peptide loops (E–F loops), which stick out from the cytoplasmic side of the PM, as previously reported by AFM[30-33].

We first performed the 3D Δf mapping of the PM under the same large amplitude condition. Since this oscillation amplitude was greater than the typical thickness of a hydration shell, which roughly corresponds to the diameter of a water molecule (0.28 nm), the frequency shift caused by the hydration structures is averaged out, thus we did not expect the hydration structure in the frequency shift curves under this condition. We rather expected to

estimate the magnitude of the direct interaction force between the tip and protein surface.

Figure 3a,b show the constant Δf images of the cytoplasmic side of the PM reconstructed with different Δf values from the 3D Δf map taken under the large amplitude condition. These images correspond to the FM-AFM topographic images with different tip-sample interaction forces. The white circles in Figure 3a,b indicate the same bR trimer. In Figure 3a, the three protruding E–F loops within each bR trimer were clearly visualized as the three bright spots. However, in Figure 3b, each bR trimer showed donut-like asymmetric structures and the three E–F loops in the bR trimers were no longer resolved as individual bright spots. We assume that the asymmetric structures in Figure 3b was observed presumably because of the non-ideal tip conditions since the experiment under the large amplitude condition was actually performed about 24 hours before the experiment in the small amplitude condition, which will be discussed later. These results obtained under the large amplitude condition indicated the deformation of bR[30,31] because of the higher tip-sample interaction force in Figure 3b (Δf = +220 Hz) than that in Figure 3a (Δf = +140 Hz). For precisely discussing the effect of the sample deformation, we extracted 5 Δf curves on the E–F loops and 960 Δf curves in the other area (whole PM) that were at chosen regardless of the area from the 3D data taken under the large amplitude condition, and averaged them as shown in Figure 3c. A single peak was clearly observed at z = 1.5 nm in the averaged Δf curve on the E–F loops, whereas the averaged Δf curve on the whole PM was monotonous. The peak value

of +160 Hz in Figure 3c was higher than the value with which the constant Δf image in Figure 3a was reconstructed (Δf = +140 Hz). Therefore, we attributed the peak to the effect of the deformation of the protruding E–F loops. The Δf curves in Figure 3c were converted into the force versus distance curves by using the formula proposed by J. E. Sader and S. P. Jarvis[34], as shown in Figure 3d. The peak Δf value on the E–F loops in Figure 3c corresponds to the force of +85 pN, from which we assumed the tip started to contact at the interaction force of +85 pN. Therefore, we defined the z-position at which the interaction force reached +85 pN as the surface position (h_0), which was slightly different for each force versus distance curve. It should be noted that it has been reported that the E–F loops deform at the force on the order of 0.1 nN[31], which is consistent with our experiment. We interpreted that Fig. 3a shows the representing the locations of the E–F loops, typical topography, while Fig. 3b shows a deformed trimer, as previously reported[31].

Next, we performed the 3D Δf mapping of the PM with the small amplitude (small amplitude condition, A = 0.12 nm) suitable for measuring the hydration structures. We analyzed the 3D Δf data, and found that the trimer contrast changes as a function of the distance as well as under the large amplitude condition but in a different manner. Figure 4a,b show the 2D Δf images in x–y planes of z = 0.8 nm and 1.5 nm (constant z images) measured on the PM, recorded under the small amplitude condition. The bright and dark contrasts reflect the repulsive and attractive interaction forces, respectively. In Figure 4a,b, trimeric

contrasts reflecting the three-fold symmetry of the bR trimers were clearly resolved. However, we found that the arrangements of the trimeric structures in Figure 4a,b were quite different, as highlighted by the white circles. To better clarify the difference in the trimeric contrast, we applied real-space lattice averaging to these images using WSxM software[35] and presented the averaged images along with the schematics below the original images. As previously discussed, the trimeric contrast near the PM surface in Figure 4a represents the locations of the E–F loops, as well as Fig. 3a. On the other hand, the trimeric contrast far from the PM surface observed at z = 1.5 nm in Figure 4b was located above the C–D loops. Figure 4c shows the 2D Δf map in the x–z plane on the PM in a vertical cross-section along the A–B line in Figure 4b, which was reconstructed from the 3D Δf map in the small amplitude condition. The white area without contrast at the bottom of the map in Figure 4c corresponds to the region where the Δf data were not recorded because of the tip retraction. In Figure 4c, vertical peaks at z = 0.8 nm were observed at regular x-intervals, which approximately corresponded to the lattice constant of the PM (6.2 nm) since the A–B line in Figure 4b was along the locations of the C–D loops in the bR trimers. We also found peaks at z = 1.5 nm, which were laterally localized at the same x-intervals. For precisely discussing these localized peaks, we extracted 5 Δf curves on the E–F loops, 9 curves on the C–D loops, and 10 curves on the centers of the bR trimers from the 3D Δf map taken under the small amplitude condition, independently averaged, and further smoothed them (Figure 5a–c). These Δf curves were then

converted into the force curves (Figure 5d–f). In the Δf curve on the E–F loops (Figure 5a), a single Δf peak was observed. The corresponding force curve in Figure 5d shows that the peak position was slightly closer but almost the same as the sample surface (h_0) where the interaction force reached +85 pN. Therefore, we concluded that this peak reflected the deformation of the protruding E–F loops, as observed in Figure 3b,d. In contrast, in the Δf curve on the C–D loops (Figure 5b), a single Δf peak was observed at z = 1.5 nm, which was 0.3 nm from the sample surface (h_0), as presented in Figure 5e.

We show the results of analysis of the same data set but for the same number of Δf curves on each region in Supplementary Fig. S1. It should be noted that the average of another set of Δf curves quantitatively matched to that presented in Fig. 5. In Fig. S1, we also show the scattering of the curves on each region, where the Δf peak at the distance of about 1 nm were consistently observed on the E–F loops but the position and the peak height were more scattered than those on the C–D loops, presumably because of the fluctuation of the E–F loop.

We found that the position of the Δf peaks on the C–D loops from 0.3 nm from h_0 under the small amplitude condition. It should be noted that h_0 was defined at the position of the force of +85 pN, which corresponds to the Δf peak on the E–F loops observed under the large amplitude mode. Namely the definition was based on the two experiments in series. In the state-of-art FM-AFM in liquids, the tip conditions still often change even during a single

experiment. Therefore we assume that there are some errors in h_0 which was defined based on the alignment of the data taken under the large and small amplitude conditions. On the other hand, we calculated the standard deviation of the absolute Δf peak positions above the C-D loops shown in Fig. S1b, and found that the standard deviation was 0.077 nm. Therefore we consider that the statistical error in the Δf peak position from h_0 (0.3 nm) was utmost 0.1 nm.

The 2D or 3D hydration structure imaging by using FM-AFM is a rather novel technique[23]. Since we first demonstrated the 2D hydration structures on bR[17], the number of the published papers on the hydration structure measurements on the biomolecules is still a few[20,21]. Not only for the hydration structure measurements on the biomolecules, many papers discuss the data set. This means that the hydration structure is obtained only when the tip apex and the hydration shell on the tip apex was in the ideal conditions and that it is unfortunately still difficult to keep the tip conditions in a single experiment and even difficult to perform the multiple experiments under the same tip conditions. While the technique is established, the tip reproducibility for the high-resolution hydration structure has not matured yet. Therefore at this moment the FM-AFM community cannot provide the statistical data on the hydration structures.

We observed the Δf peaks on the C–D loops before the Δf peaks on the E–F loops due to the deformation when the tip was approached, despite that the E–F loops are protruded from other loops and domains as schematically shown in the cartoon in Fig. 4c and

experimentally observed as well, as shown in Fig. 3. We also took into account the fact that the Δf peaks on the C–D loops were not observed under the large amplitude mode. Therefore we concluded that the Δf peaks on the C–D loops should be attributed to the water molecules, not the deformation of the C–D loops. It should also be noted that uncertainty and variance of the height of the Δf peaks from the sample surface does not significantly affect the main conclusion.

Finally, the Δf and force curves on the centers of the bR trimers (Figure 5c,f) were almost monotonous and no peaks or shoulders were observed. This strongly suggests that the peaks in the Δf and force curves in Figure 5b,e were originating from the highly localized hydration forces.

FM-AFM can only detect the hydration structures that are stable during a timescale of an oscillation period, in this case on the order of a microsecond, but are easily perturbed by the tip. Moreover, the structures of the loops and domains should not be fluctuating. Since we only observed the hydration structures on the C-D loops in this experiment, we presume that the hydration structures as well as the mechanical structures of the C-D loops are relatively stable compared to the other loops and domains. It should be noted that the hydration shells observed on the C-D loops are characterized as one-dimensional spots, which represent that the hydration shells on the C-D loops are considered as confined not only in the vertical direction but also in the lateral direction[24].

We performed the experiments in a high ionic concentration to shorten the Debye length both on the tip and sample sides and reduce the effect of a long-range electric double layer force on the experiment[19,22,25,26]. In the previous experiment on muscovite mica in a high ionic concentration[19], we did not observe the adsorbed ions. In this experiment, we also did not observe any adsorbed ions. However, the Δf peaks observed on the C–D loops may be attributed to the solvation force of the hydrated ions. It should be noted that the cytoplasmic side of the purple membrane of the archaea *Halobacterium salinarum* is usually exposed to a saturated NaCl solution, the concentration of 3 M KCl is rather suitable for investigation of the natural hydration structures rather than a pure water.

In summary, we have successfully visualized localized hydration structure on the C–D loops on the cytoplasmic side of the bR. The residue Asp-96, which is directly involved in proton transfer, is located in the C-helix near the cytoplasmic side of the bR[36]. Hence, localized water molecules near the C–D loops may contribute to the proton translocation on the cytoplasmic side of the bR. Not only the accumulation of the 3D force map data of a high quality as presented here, a comparison with the theoretical studies regarding the water distributions around the proteins, such as by a molecular dynamics simulation[37] or molecular Ornstein–Zernike theory[38], is also necessary for further interpretation of the 3D force mapping results. Recently, we demonstrated the measurement of the dynamical nature of the hydration structures (viscosity) on an inorganic substrate through the dissipation measurement by using

FM-AFM[39]. In a near future we will investigate the dynamical nature of the hydration structures on the biomolecules as well.

In conclusion, we have presented the 3D Δf mapping of the PM by FM-AFM. From the 3D Δf map of the PM under the large amplitude condition (A = 0.5 nm), the tip-sample interaction force that caused deformation of the PM was estimated (F = +85 pN). From the 3D Δf map under the small amplitude condition (A = 0.12 nm), the Δf peaks laterally localized on the C–D loops were observed. By excluding the effect of sample deformation observed in the large amplitude condition, we concluded that these peaks were caused by the local hydration structures on the bR. The localization of water molecules near the C–D loops observed in this study may play important roles in the light-driven proton pump of the bR proteins. Our results are important for structure-function considerations of general pump proteins in solution. Moreover, the 3D Δf mapping by FM-AFM will be widely applicable to the molecular-scale investigations of solid-liquid interfaces of various soft nanomaterials.

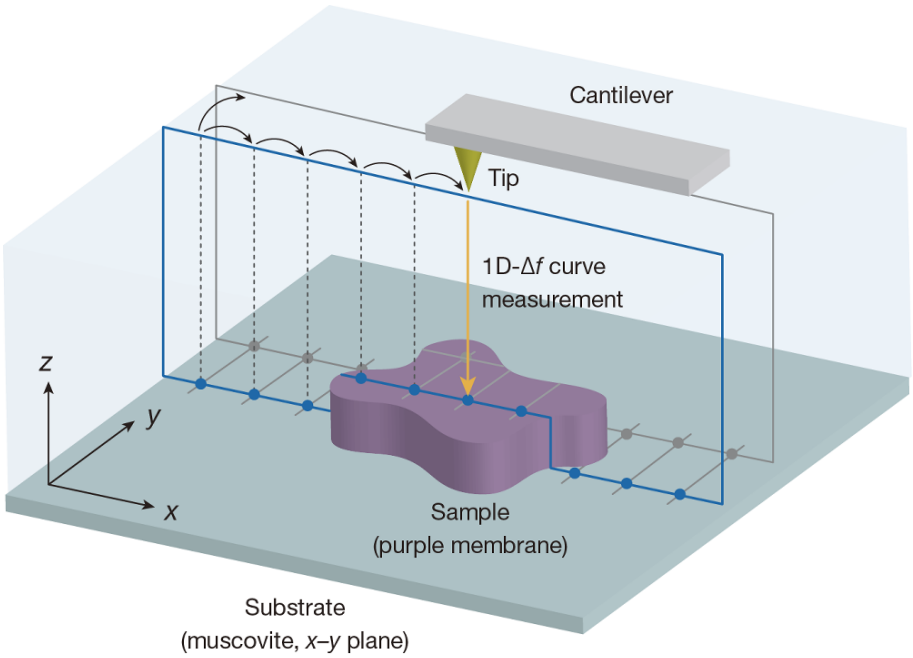

Figure 1. Schematic diagram of the 3D frequency shift mapping by the FM-AFM. A 2D rectangular grid was allocated to a substrate (*x*–*y* plane), and the frequency shift of a cantilever (Δf) was recorded at each intersection of the grid, which corresponded to the scanning pixels, while translating an AFM tip in the *z*-direction for the Δf versus distance curve measurements. The minimum tip-sample distance at each pixel was regulated by placing an upper limit (Δf threshold) on the frequency shift.

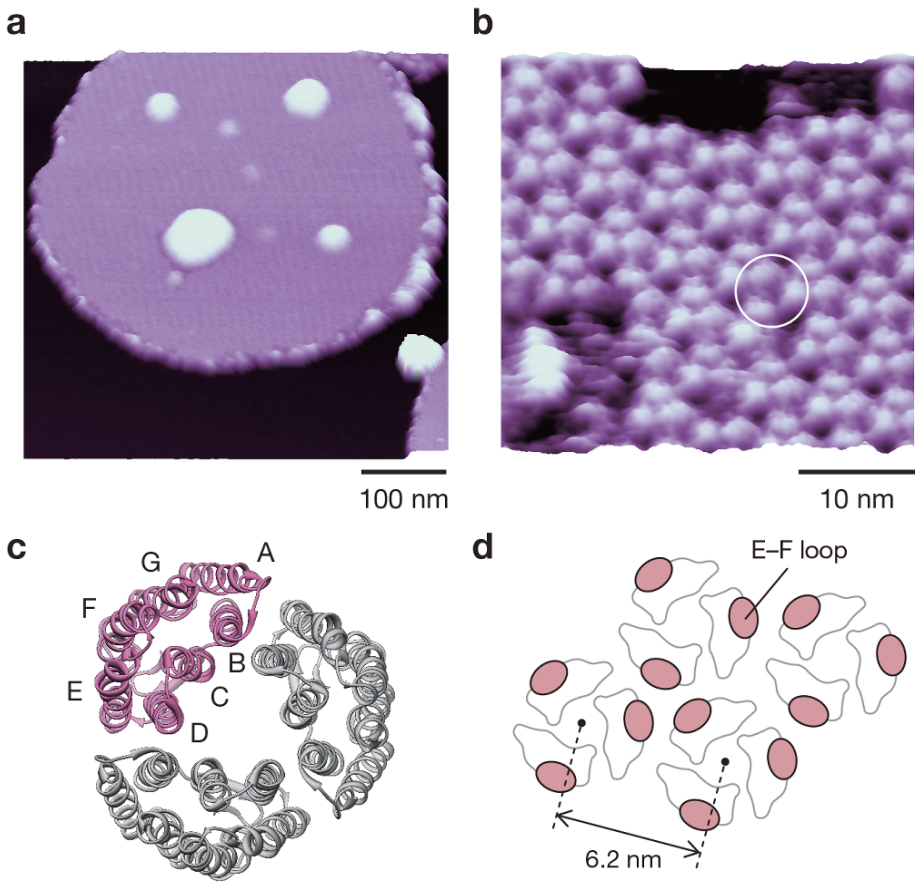

Figure 2. (a–b) Typical FM-AFM topographic images of the cytoplasmic side of the purple membrane showing the 2D crystals of bacteriorhodopsin (bR) in an aqueous solution (3 M KCl). The white circle in (b) indicates an individual bR trimer. (c) Molecular structure of a bR trimer (cytoplasmic side, PDB ID code: 1FBB). The 7 transmembrane alpha-helices of bR connected by peptide loops were labeled as A–G helices. (d) Model of the cytoplasmic side of the bR trimers. The red regions indicate the positions of the protruding E–F loops, which correspond to the bright spots in the AFM image in (b).

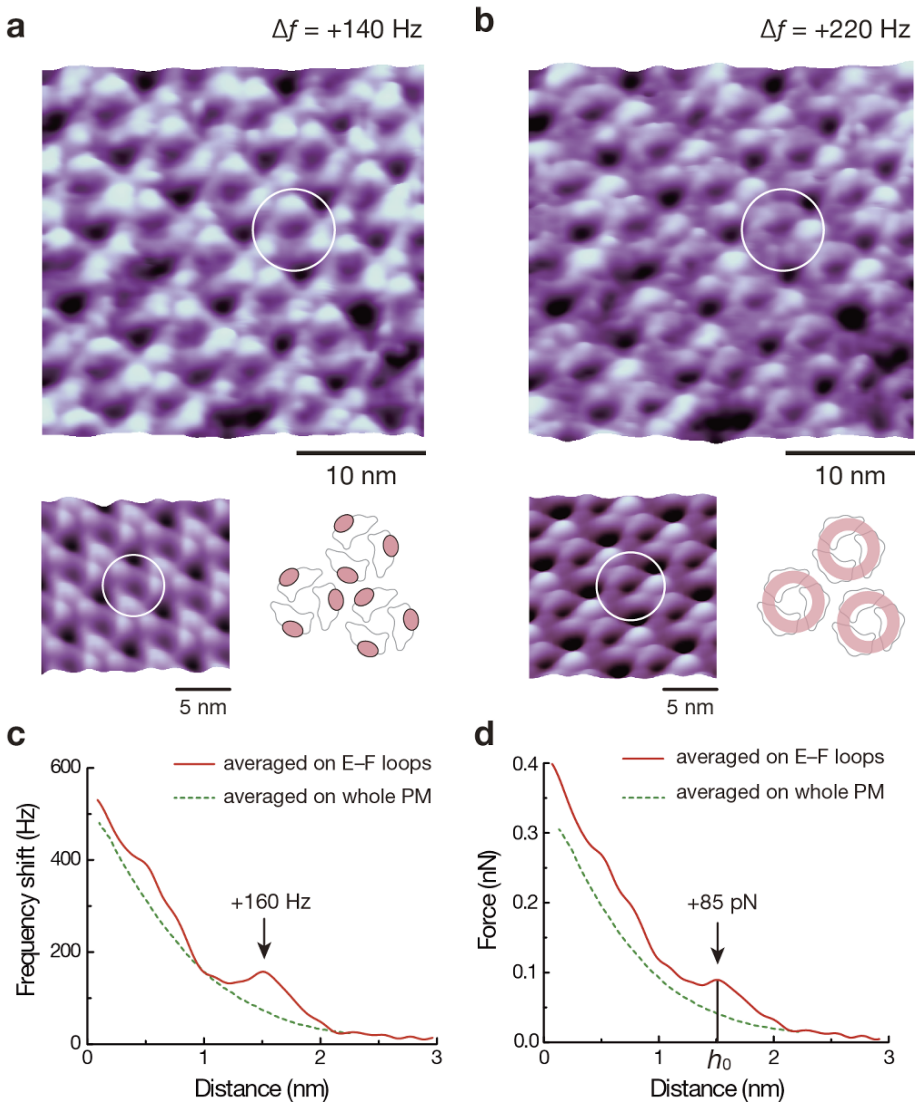

Figure 3. 3D Δf mapping of the cytoplasmic side of the PM in an aqueous solution (3M KCl) with the oscillation amplitude of 0.5 nm. (a–b) Constant Δf images (topographic images) with different tip-sample interaction forces reconstructed from the 3D Δf map. The white circles indicate the individual bR trimers. (c) Δf curves averaged on the E–F loops (solid line) and on random pixels of the PM (dotted line) in the 3D Δf map. (d) Force versus distance curves (force curves) converted from the Δf curves in (c).

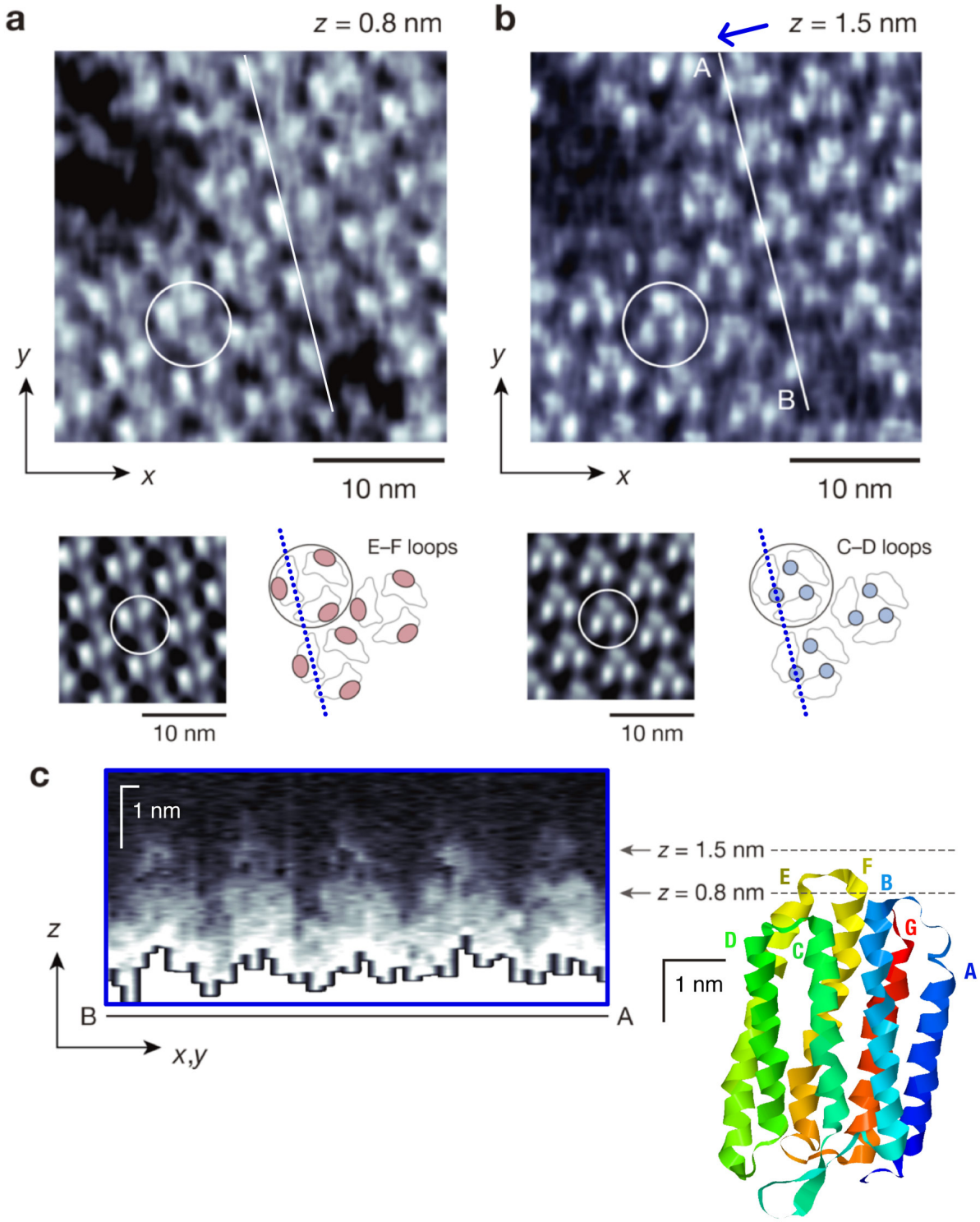

Figure 4. 2D Δf maps extracted from the 3D Δf map on the cytoplasmic side of the PM in an aqueous solution (3 M KCl) with the oscillation amplitude of 0.12 nm. (a–b) 2D Δf maps in the x–y planes (constant z images) in the horizontal cross-sections with different z-positions extracted from the 3D Δf map. The trimeric structures with different arrangements are

indicated by the white circles. The images after the real-space lattice averaging and the schematics of the trimeric contrasts are also shown. (c) 2D Δf map in the x–z plane along the A–B line in Figure 4b extracted from the 3D Δf map. The 2D map shows the Δf data in the cross-section along the C–D loops, as seen from the viewpoint as indicated by the arrow. The image size is 28 nm × 4 nm. A cross-sectional cartoon of a bR monomer is also presented in the same vertical scale but in a different horizontal scale from that of the 2D map. The cartoon was drawn based on the structural data in the Protein Data Bank (PDB ID code: 1FBB). The topmost atom in the E–F loop was aligned at the height of 1.2 nm, such that the bright spots corresponding to the Δf peaks in the 2D Δf map are positioned at z = 1.5 nm.

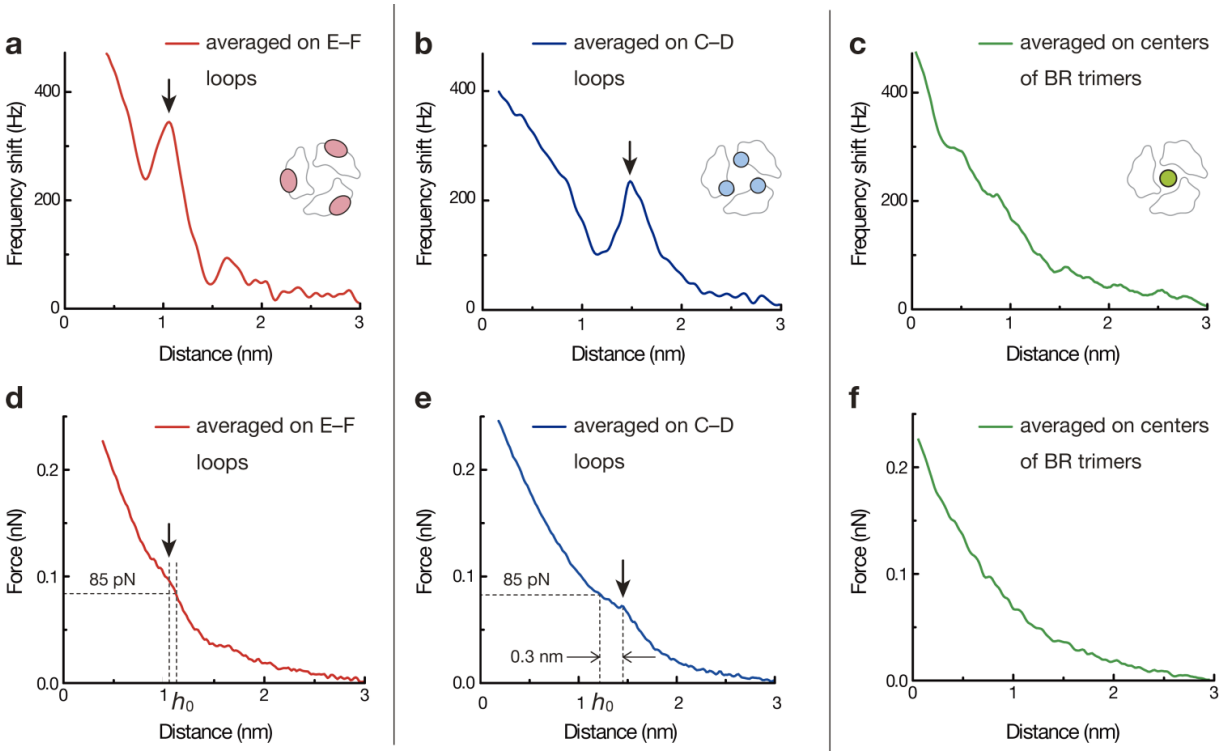

Figure 5. Δf curves extracted from the 3D Δf map on the cytoplasmic side of the PM in an aqueous solution (3 M KCl) with the oscillation amplitude of 0.12 nm and corresponding force curves. (a) Averaged Δf curve on the E–F loops. (b) Averaged Δf curve on the C–D loops. (c) Averaged Δf curve on the centers of the bR trimers. (d–f) Force curves converted from the Δf curves in (a–c).

METHODS

FM-AFM setup. We used a customised AFM instrument (SPM-9600, Shimadzu) with a home-built digital controller using a field-programmable gate array module programmed in LabVIEW (National Instruments). The noise-equivalent displacement noise density was reduced to approximately 5–10 fm/√Hz by modification of the optics and electronics in the cantilever deflection sensor. We used a highly-doped Si cantilever with an Au coating on the backside (PPP-NCHAuD, Nanosensors). The nominal spring constant of the cantilever was 42 N/m. The resonance frequency and quality factor in the solution were about 130 kHz and 7, respectively. A phase locked loop circuit with a voltage controlled crystal oscillator was used to detect the frequency shift. An automatic gain control circuit kept the oscillation amplitude of the cantilever constant. The same cantilever (AFM tip) was used for all FM-AFM measurements in this study. In order to reduce thermal drift in the FM-AFM system, ambient temperature was kept constant at 20°C by setting the FM-AFM instrument in an incubator (CN-40A; Mitsubishi Electric Engineering).

Sample preparation. 20 μl droplet of the PM suspension (0.5 μM) was deposited onto a freshly cleaved mica substrate (1 cm × 1 cm, Furuuchi Chemical). Ten minutes later, the substrate was gently rinsed three times with buffer solution (10 mM phosphate buffer solution: PBS, pH7.4) containing 3 M potassium chloride (KCl). We performed the FM-AFM

imaging and 3D Δf mapping in the same 3 M KCl solution before drying it.

3D frequency shift mapping. Each 2D frequency shift map was collected in the z–x plane with dimensions of 29.8 nm (192 pixels) in z direction by 4.2 nm (256 pixels) in the x direction. At each x position, 1D frequency shift curve was recorded while the tip was approached to the sample surface with a tip velocity of 400 nm/s by applying a ramp signal of 48 Hz. The ramp signal was immediately stopped when the frequency shift signal reached a predetermined threshold value, +630 Hz in this case, and the tip was retracted to the original position (See Supporting Information). By employing the tip retraction function, 64 slices of 2D frequency shift maps were obtained in 490 seconds without damage to the sample.

SUPPORTING INFORMATION

This material is available free of charge via the internet at http://pubs.acs.org.

Site-specific frequency shift curves, description of tip retraction function, and AFM image of damaged purple membrane.

AUTHOR INFORMATION

Corresponding Author

*E-mail: h-yamada@kuee.kyoto-u.ac.jp

Author contributions

S.I. performed AFM imaging, analyzed data, and wrote the paper. N.O. programmed the AFM controller software and assisted in AFM imaging. K.K. developed AFM instruments and electronics, and wrote the paper. Y. H. prepared the biological sample. K.M. designed the study. H.Y designed the study, developed AFM instruments, analyzed the data, and wrote the paper. All authors have discussed the results and commented on the manuscript.

Notes

The authors declare no competing financial interest.

ACKNOWLEDGMENTS

The authors would like to acknowledge Dr. Hirofumi Sato, Dr. Daisuke Yokogawa, and Mr.

Kenji Hirano for helpful discussions. This work was supported by KAKENHI, Japan Society for the Promotion of Science (17H06122 and 19H02598), SENTAN Program of the Japan Science and Technology Agency, and Global COE Program of the Japanese Society for the Promotion of Science. S.I. was supported by the Japan Society for the Promotion of Science Fellowship.

REFERENCES

1 Levy, Y. & Onuchic, J. N. Water mediation in protein folding and molecular recognition. *Annu. Rev. Biophys. Biomol. Struct.* **35**, 389-415 (2006).

2 Chaplin, M. Do we underestimate the importance of water in cell biology? *Nat. Rev. Mol. Cell Biol.* **7**, 861-866 (2006).

3 Kandori, H. Role of internal water molecules in bacteriorhodopsin. *Biochim. Biophys. Acta* **1460**, 177-191 (2000).

4 Lanyi, J. K. Bacteriorhodopsin. *Annu. Rev. Physiol.* **66**, 665-688 (2004).

5 Haupts, U., Tittor, J. & Oesterhelt, D. Closing in on bacteriorhodopsin: progress in understanding the molecule. *Annu. Rev. Biophys. Biomol. Struct.* **28**, 367-399 (1999).

6 Oesterhelt, D. & Stoeckenius, W. Rhodopsin-like protein from the purple membrane of *Halobacterium halobium*. *Nature* **233**, 149-152 (1971).

7 Henderson, R. & Unwin, P. N. Three-dimensional model of purple membrane

obtained by electron microscopy. *Nature* **257**, 28-32 (1975).

8 Khorana, H. G. *et al.* Amino acid sequence of bacteriorhodopsin. *Proc. Natl. Acad. Sci. USA* **76**, 5046-5050 (1979).

9 Zaccai, G. Moist and soft, dry and stiff: a review of neutron experiments on hydration-dynamics–activity relations in the purple membrane of *Halobacterium salinarum*. *Biophys. Chem.* **86**, 249-257 (2000).

10 Binnig, G., Quate, C. F. & Gerber, C. Atomic force microscope. *Phys. Rev. Lett.* **56**, 930-933 (1986).

11 Müller, D. J., Janovjak, H., Lehto, T., Kuerschner, L. & Anderson, K. Observing structure, function and assembly of single proteins by AFM. *Prog. Biophys. Mol. Biol.* **79**, 1-43 (2002).

12 Müller, D. J. & Dufrene, Y. F. Atomic force microscopy as a multifunctional molecular toolbox in nanobiotechnology. *Nat. Nanotech.* **3**, 261-269 (2008).

13 Müller, D. J. *et al.* Atomic force microscopy of native purple membrane. *Biochim. Biophys. Acta* **1460**, 27-38 (2000).

14 Shibata, M., Yamashita, H., Uchihashi, T., Kandori, H. & Ando, T. High-speed atomic force microscopy shows dynamic molecular processes in photoactivated bacteriorhodopsin. *Nat. Nanotech.* **5**, 208-212 (2010).

15 Albrecht, T. R., Grütter, P., Horne, D. & Rugar, D. Frequency modulation detection

using high-*Q* cantilevers for enhanced force microscope sensitivity. *J. Appl. Phys.* **69**, 668-673 (1991).

16 Fukuma, T., Kobayashi, K., Matsushige, K. & Yamada, H. True atomic resolution in liquid by frequency-modulation atomic force microscopy. *Appl. Phys. Lett.* **87**, 034101 (2005).

17 Kimura, K. *et al.* Visualizing water molecule distribution by atomic force microscopy. *J. Chem. Phys.* **132**, 194705 (2010).

18 Suzuki, K., Oyabu, N., Kobayashi, K., Matsushige, K. & Yamada, H. Atomic-resolution imaging of graphite-water interface by frequency modulation atomic force microscopy. *Appl. Phys. Express* **4**, 5102 (2011).

19 Kobayashi, K. *et al.* Visualization of hydration layers on muscovite mica in aqueous solution by frequency-modulation atomic force microscopy. *J. Chem. Phys.* **138**, 184704 (2013).

20 Asakawa, H., Yoshioka, S., Nishimura, K. I. & Fukuma, T. Spatial Distribution of Lipid Headgroups and Water Molecules at Membrane/Water Interfaces Visualized by Three-Dimensional Scanning Force Microscopy. *ACS Nano* **6**, 9013-9020 (2012).

21 Herruzo, E. T., Asakawa, H. Fukuma, T. & Garcia, R. Three-dimensional Quantitative Force Maps in Liquid with 10 Piconewton, Angstrom and Sub-minute Resolutions. *Nanoscale* **5**, 2678-2685 (2013).

22 Umeda, K. *et al.* Atomic-resolution three-dimensional hydration structures on a heterogeneously charged surface, *Nat. Commun.* **8**, 2111 (2017).

23 Fukuma, T. & Garcia, R. Atomic- and Molecular-Resolution Mapping of Solid−Liquid Interfaces by 3D Atomic Force Microscopy. *ACS Nano* **12**, 11785-11797 (2018).

24 Umeda, K., Kobayashi, K., Minato, T. & Yamada, H. Atomic-Scale 3D Local Hydration Structures Influenced by Water-Restricting Dimensions. Langmuir 34, 9114-9121 (2018).

25 Suzuki, K., Kobayashi, K., Oyabu, N., Matsushige, K. & Yamada, H. Molecular-scale investigations of structures and surface charge distribution of surfactant aggregates by three-dimensional force mapping. *J. Chem. Phys.* **140**, 054704 (2014).

26 Umeda, K., Kobayashi, K., Oyabu, N., Matsushige, K. & Yamada, H. Molecular-scale quantitative charge density measurement of biological molecule by frequency modulation atomic force microscopy in aqueous solutions. *Nanotechnol*. **26**, 285103 (2015).

27 Giessibl, F. J. Advances in atomic force microscopy. *Rev. Mod. Phys.* **75**, 949-983 (2003).

28 Subramaniam, S. & Henderson, R. Molecular mechanism of vectorial proton translocation by bacteriorhodopsin. *Nature* **406**, 653-657 (2000).

29 Pettersen, E. F. et al. UCSF Chimera – a visualization system for exploratory research

and analysis. *J. Comput. Chem.* **25**, 1605-1612 (2004).

30 Medalsy, I., Hensen, U. & Muller, D. J. Imaging and quantifying chemical and physical properties of native proteins at molecular resolution by force-volume AFM. *Angew. Chem. Int. Ed.* **50**, 12103-12108 (2011).

31 Hoogenboom, B. W., Hug, H. J., Pellmont Y., Martin, S., Frederix, P. L. T. M., Fotiadis, D. & Engel, A. Quantitative dynamic-mode scanning force microscopy in liquid. *Appl. Phys. Lett.* **88**, 193109 (2006).

32 Müller, D. J., Sass, H. J., Müller, S. A., Büldt, G. & Engel, A. Surface structures of native bacteriorhodopsin depend on the molecular packing arrangement in the membrane. *J. Mol. Biol.* **285**, 1903-1909 (1999).

33 Yamada, H. *et al.* Molecular resolution imaging of protein molecules in liquid using frequency modulation atomic force microscopy. *Appl. Phys. Express* **2**, 95007 (2009).

34 Sader, J. E. & Jarvis, S. P. Accurate formulas for interaction force and energy in frequency modulation force spectroscopy, *Appl. Phys. Lett.* **84**, 1801-1803 (2004).

35 Horcas, I. & Fernández, R. WSXM: A software for scanning probe microscopy and a tool for nanotechnology, *Rev. Sci. Instrum.* **78**, 013705 (2007).

36 Greenhalgh, D. A., Altenbach, C., Hubbell, W. L. & Khorana, H. G. Locations of Arg-82, Asp-85, and Asp-96 in helix C of bacteriorhodopsin relative to the aqueous boundaries. *Proc. Natl. Acad. Sci. USA* **88**, 8626-8630 (1991).

37 Reischl, B., Watkins, M. & Foster, A. S. Free energy approaches for modeling atomic force microscopy in liquids. *J. Chem. Theory Comput.* **9**, 600-608 (2013).

38 Yokogawa, D., Sato, H. & Sakaki, S. The position of water molecules in Bacteriorhodopsin: a three-dimensional distribution function study. *J. Mol. Liq.* **147**, 112-116 (2009).

39 Umeda, K., Kobayashi, K., Minato, T. & Yamada, H. Atomic-Level Viscosity Distribution in the Hydration Layer. Phys. Rev. Lett. 122, 116001 (2019).

TOC GRAPHIC

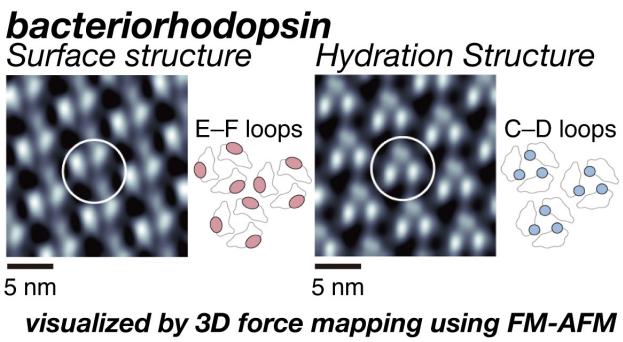
bacteriorhodopsin
Surface structure
Hydration Structure
E–F loops
C–D loops
5 nm
5 nm
visualized by 3D force mapping using FM-AFM